The angular range of effective pinning by one-dimensional artificial pinning centers in $BaZrO_3$/$YBa_2Cu_3O_{7-x}$ nanocomposite films

Victor Ogunjimi (iD), Bibek Gautam (iD), Mary Ann Sebastian (iD), Timothy Haugan, and Judy Wu

View Online   **Export Citation**   **CrossMark**

ARTICLES YOU MAY BE INTERESTED IN

NEW

AVS Quantum Science

A new interdisciplinary home for impactful quantum science research and reviews

Co-Published by AIP Publishing / AVS

NOW ONLINE

The angular range of effective pinning by one-dimensional artificial pinning centers in BaZrO₃/YBa₂Cu₃O₇₋ₓ nanocomposite films

View Online   Export Citation   CrossMark

Victor Ogunjimi,[1,a]   Bibek Gautam,[1]   Mary Ann Sebastian,[2,3]   Timothy Haugan,[2]   and Judy Wu[1]

AFFILIATIONS

[1] Department of Physics and Astronomy, the University of Kansas, Lawrence, Kansas 66045, USA
[2] U.S Air Force Research Laboratory, Aerospace Systems Directorate, WPAFB, Ohio 45433, USA
[3] University of Dayton Research Institute, Dayton, Ohio 45469, USA

[a] victorogunjimi@ku.edu

ABSTRACT

Nanoscale c-axis-aligned one dimensional artificial pinning centers (1D-APC) in superconducting YBa₂Cu₃O₇₋ₓ (YBCO) films have been shown to provide strong correlated pining to magnetic vortices at magnetic field $H//c$-axis. A question arises on how the pinning effectiveness is sustained as the H-orientation (θ) deviates from the c-axis and how such an angular range is correlated to the pinning efficiency of an individual 1D-APC. To shed lights on this question, this work investigates the angular range of pinning effectiveness of the BaZrO₃ (BZO) 1D-APCs in BZO/YBa₂Cu₃O₇₋ₓ nanocomposites as the strain field overlap is systematically varied by increasing the BZO doping level in the range of 2-6 vol.% and by the introduction of the secondary Y₂O₃ nanoparticles (3D APCs). By evaluating the maximum pinning force density ($F_{p, max}$), its location H_{max}, and the α values of the nanocomposites normalized to that of the reference YBa₂Cu₃O₇₋ₓ film as functions of θ at temperatures of 65–77 K, a quantitative correlation between the pinning efficiency of the BZO 1D-APCs and their effective angular range was obtained. In most samples, the 1D-APCs can provide enhanced H_{max} in the range of $\theta \sim 0°$-$60°$. However, the $F_{p, max}$ values only in nanocomposites with high pinning efficiency 1D-APCs exceed that of the YBa₂Cu₃O₇₋ₓ over a smaller range up to $\theta \sim 37°$. Finally, the introduction of 3D APCs results in reduction of the α values over nearly the entire angular range. This study reveals the importance in improving individual 1D-APC's pinning efficiency and hence extending its angular range of effective pinning.

I. INTRODUCTION

Over the last decade or so, nanoscale artificial pinning centers (APCs) of a variety of morphologies have been reported in superconducting YBa₂Cu₃O₇₋ₓ (YBCO) films on dielectric or metal substrates for enhancement of magnetic vortex pinning and hence critical current density J_c in applied magnetic fields (H). Among others, c-axis-aligned one-dimensional APCs, or 1D-APCs, have shown to provide strong correlated pinning at $H//c$-axis. This is particularly important for layer-structured YBCO, with its strong anisotropy of $J_c(H)$ (with respect to the orientation of the magnetic field), due to lack of strong pins along the c-axis in contrast to the strong intrinsic pinning at $H//ab$-plane.[1,2] The addition of the c-axis aligned 1D-APCs

in YBCO films has been shown to lead to remarkably enhanced pinning at $H//c$-axis of the 1D APC/YBCO nanocomposite films. The first reported APC study on BaZrO₃ (BZO) doped YBCO films was conducted by MacManus-Driscoll *et al* BZO doped YBCO films, which demonstrated a 5-fold improvement of J_c at 75.5 K and 7 T indicating enhanced pinning by the BZO APCs.[3] This initiated many interesting works on generation of APCs and characterization of the pinning enhancement. Several insulator dopants are demonstrated to form 1D-APCs in YBCO through strain-mediated self-assembly during growth[4,5] including BaZrO₃ (BZO), BaSnO₃(BSO), BaHfO₃ (BHO)[6–15] and Ba₂Y(Nb/Ta)O₆.[15–17] Considering the 1D-APCs are effective only within a certain angular range around $H//c$-axis, doping of APCs of mixed morphologies has been explored

recently for strong, as well as isotropic pinning at all orientations of the magnetic field, to meet the specifications of applications in high-field magnets, motors, generators, transformers, etc.[5,18–24] For example, the secondary dopant, Y_2O_3, typically forms 3D APCs and can be combined with the primary BZO (BHO or BSO) 1D- APCs to form 1D+3D APC/YBCO nanocomposite films to reduce the H-orientation dependence of J_c.[7,20,23,25–30]

A quantitative understanding of the pinning efficiency of APCs is important to the design of an optimal pinning landscape in APC/YBCO nanocomposite films.[31] A particular question regarding the 1D-APCs is to what extent of the angular range of the magnetic field the 1D-APCs can retain their pinning effectiveness in single-doped 1D-APC/YBCO nanocomposites and how this angular range correlate with the pinning efficiency of individual 1D-APC quantitatively? In order to answer this question, $J_c(H)$ curves were measured at different magnetic field orientations, defined with the angle θ in the plane perpendicular to J_c with $\theta=0°$ at $H//c$-axis and $\theta=90°$ at $H//ab$-plane. Figure 1 is a schematic diagram illustrating the deviation (θ) of the magnetic field direction from the c-axis of YBCO ($\theta=0$ at $H//c$-axis). This study differs from the $J_c(\theta)$ measurement at a fixed magnetic field since the pinning efficiency of a 1D-APC depends sensitively on the magnetic fields.[3,23,32–38] Civale and Maiorov et al have effectively demonstrated the usefulness of $J_c(\theta)$ studies in identifying and comparing the pinning landscapes.[23] However, the sensitivity of this approach to the applied magnetic field is better illuminated by the Shihong Chen et al study on 6 vol.% BZO doped YBCO at 77 K and 65 K. They reported $J_c(\theta)$ profiles with J_c anisotropy, defined from $(J_{c,max} - J_{c,min}/J_{c,min})$, of 100%, 150%, and 483% at 1 T, 3 T and 5 T respectively at 77 K. The J_c anisotropy values were reduced to 70% and 96% at 5 T and 9 T respectively at 65 K.[26] This clear dependence on field and temperature makes drawing pinning conclusions using $J_c(\theta)$ data quite challenging. In this study, this field dependence was bypassed by calculating the pinning force density ($F_p(H) = J_c \times H$) at different orientations of the magnetic field for a direct comparison with the reference YBCO case. By plotting the F_p peak value ($F_{p,max}$) and location (H_{max}) of the nanocomposite samples normalized to that of YBCO as functions of θ, we aim to elucidate a quantitative

correlation between pinning efficiency of individual 1D-APCs and their angular pinning effectiveness. In addition, fitting the $J_c(H)$ curves with $J_c \sim H^{-\alpha}$ allows the extraction of the α values as a function of θ.[39,40]

II. EXPERIMENT

A set of BZO doped YBCO samples were selected for this study. They include 2, 4, and 6 vol.% singly-doped BZO/YBCO nanocomposite films (to be regarded henceforth also as 2%, 4% and 6% SD samples respectively) and a 4 vol.% BZO 1D-APC+3% Y_2O_3 3D APC/YBCO (to be regarded henceforth also as 4% DD sample). In addition, an undoped YBCO film was also included in the study as the reference sample. In the SD samples, only c-axis aligned BZO 1D- APCs are present and the spacing between the 1D-APCs decreases with increasing BZO doping. The variation of the inter 1D-APC spacing implies a variation of areal density (n) of the 1D-APCs in the ab-plane and therefore the matching field $B^* = n\Phi_o$ (where Φ_o is the flux quantum). In addition, the spacing would also result in an impact on the strain field distribution in the APC/YBCO nanocomposite films and hence the pinning efficiency of the individual 1D-APCs.[31,41] The 4% DD sample has APCs of mixed morphologies of 1D BZO APCs and 3D APCs.

The BZO SD and BZO DD samples were fabricated using pulsed laser deposition (PLD) on (100) $SrTiO_3$ (STO) single crystal substrates using the optimal PLD conditions identified in our previous works.[42,43] The full details of sample fabrication have been reported elsewhere.[26,44] Briefly, the substrate temperature of 825 °C in 300 mTorr oxygen were employed for PLD of the SD and DD samples. The thickness of the samples was ~ 140 nm. After the PLD deposition, the films were annealed at 500 °C in oxygen for 30 minutes. The microstructure and crystallinity of the samples were analyzed using x-ray diffraction (XRD) using a Bruker D8 diffractometer (Cu-kα wavelength 1.54 Å) and transmission Electron Microscopy (TEM). Standard photolithography was applied to pattern two microbridges of length of 500 μm and width of 20 μm and 40 μm, respectively, on each sample. Transport J_c was measured as functions of magnetic field H (0-9 T), temperature T (65 K and 77 K) and the field orientation θ in a Physical Property Measurement System (Evercool II, Quantum Design). For this experiment, θ was varied from $\theta = 0°$ ($H//c$-axis) to $\theta = 90°$ ($H//ab$-plane). The 1 μVcm^{-1} criterion was used to determine J_c from the I-V characteristic.

III. RESULTS AND DISCUSSIONS

Figure 2 shows the XRD θ -2θ spectra of the 2% BZO SD, 4% BZO SD and 6% BZO SD nanocomposite films. For a comparison, the XRD θ -2θ spectrum taken on an undoped YBCO reference sample is also include in Figure 1. The two unlabeled small peaks at $2\theta \sim 42°$ and 45° in the pristine YBCO film may be attributed to common impurity phase of Y_2O_3. The bump seen at high angles is probably due to the amorphous glass slide used as sample holder based on our calibration. Since the (00l) STO peaks almost overlap with some of those of YBCO's such as (003) and (006) peaks, these peaks have been indexed to both with a comma. The unindexed peaks in the BZO SD samples (i.e. $2\theta \sim 42°$ in 4% BZO SD) could be attributed to impurity phase of YBa_2ZrO_6 (YBZO).[45,46] On
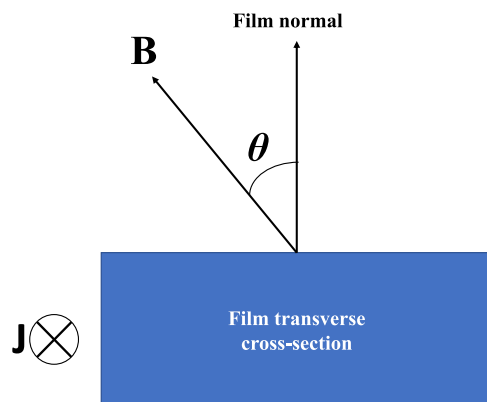

FIG. 1. Schematic showing the deviation θ of the magnetic field, B away from the c-axis direction (direction of film growth); and the direction of the flow of current in the film.
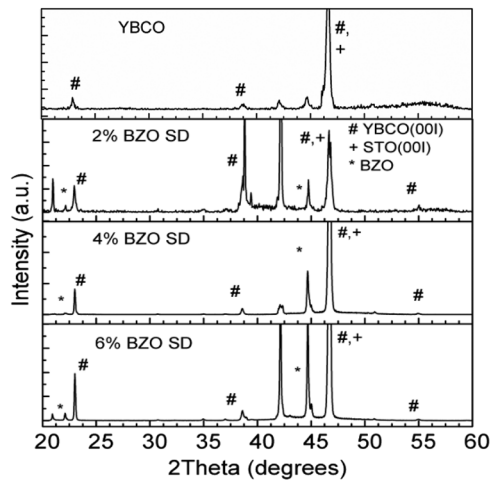
FIG. 2. XRD θ-2θ spectra for the undoped YBCO, 2% BZO SD, 4% BZO SD and 6% BZO SD nanocomposite films on STO substrates.

FIG. 3. TEM images of 2%, 4%, 6% BZO SD (a, b, c); and 4% BZO DD (d) films at low magnification.

all four samples, YBCO (00l) peaks can be clearly seen, confirming high crystallinity of these films with c-axis orientation along the normal direction of the films. Based on the (00l) peaks, the c-axis lattice constants can be calculated for the four samples in Figure 2 and the result is summarized in Table I.

In the three SD samples, the BZO (00l) peaks (*) are illustrated and the intensity of the BZO peaks increase with BZO doping. This indicates the epitaxial relationship between BZO and YBCO. The c-axis of YBCO is 11.82 Å in the 2% BZO SD sample, which is considerably higher than the 11.70 Å for the reference YBCO. This can be attributed to the tensile strain on the YBCO c-axis via formation of the c-axis aligned BZO 1D-APCs of a larger lattice constant. However, a further increase in the BZO concentration causes a reduction in the c-axis lattice constant to 11.71 Å and 11.67 Å, respectively, in the 4% and 6% BZO SD samples. This suggests a reduction of the tensile strain along the c-axis of the YBCO in the BZO SD samples at higher BZO doping most probably due to the formation of defects in YBCO lattice, via ab-plane buckling, as the strain field overlaps.[9,10,41] Interestingly, the c-axis lattice constant of 11.72 Å in 4% BZO DD sample is comparable to that of 4% BZO SD sample (Table I).[26] This suggests the c-axis tensile strain on the YBCO lattice is primarily
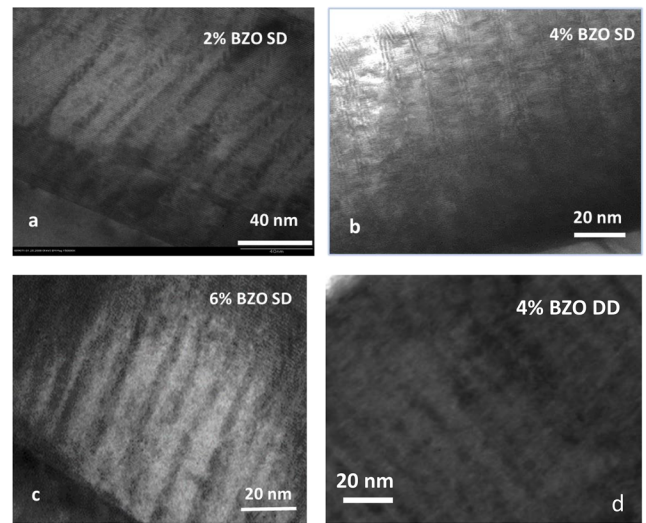
determined by the concentration of the BZO 1D-APCs. The tensile strain along the c-axis and the defects on the YBCO lattice lead to reduced superconducting critical temperatures (T_c) in the BZO SD and BZO DD samples as shown in Table I. Specifically, the T_c values are 89.27 K, 87.48 K and 86.90 K respectively for 2, 4, and 6% BZO SD films, in contrast to the T_c of ~90.0 K for the reference YBCO film. Again, the 4% BZO DD sample has T_c ~87.69 K is comparable to that of the 4% BZO SD sample.

Figures 3 includes the TEM images of the cross sections of the 2% (Figure 3a), 4% (Figure 3b), and 6% (Figure 3c) BZO SD and 4% BZO DD (Figure 3b) nanocomposite films. The c-axis aligned BZO 1D-APCs can be clearly seen in all samples. However, they are continuous through the film thickness in SD samples while some of the BZO 1D APCs become segmented in the DD samples most probably due to the perturbation of the local strain by the addition of Y_2O_3 that form 3D APCs or nanoparticles.[4,5] Consequently, a mixed morphology of 1D+2D+3D APCs was observed in the BZO DD films.[7,47] With increasing BZO concentrations, the lateral dimension of the BZO 1D-APCs is found to increase slightly from 5.2 nm

TABLE I. Summary of relevant parameters in the five samples used in this manuscript including c-axis lattice constants, superconducting transition temperature T_c, BZO 1D-APC diameter and spacing, matching field B^* and α values.

Sample ID	c-axis lattice Constant (Å)	T_c (K)	1D APC diameter (nm)	1D APC Spacing (nm)	B^* (T)	Alpha (α) at 77 K $H//c$	$H//ab$
undoped YBCO	11.70	90.00	NA	NA	NA	0.35	0.30
2 vol.% BZO SD	11.82	89.27	5.2	20.0	5.2	0.28	0.37
4 vol.% BZO SD	11.71	87.48	5.8	15.0	9.2	0.28	0.53
6 vol.% BZO SD	11.67	86.90	5.9	12.0	14.3	0.28	0.36
4 vol.% BZO DD	11.72	87.69	5.6	15.0	9.2	0.31	0.19

in 2%, to 5.8 nm in 4%, and to 5.9 nm in the 6% BZO SD samples (Table I). This increase in the lateral dimension of the BZO 1D-APCs can be explained as the consequence of the increasing strain field overlap with increasing BZO doping using an elastic strain energy model.[48,49] The average center-to-center spacing (d) between the BZO 1D-APCs can be estimated from the TEM images and the d is found to decrease linearly with increasing BZO doping from about 20 nm in the 2%, to 15 nm in the 4% and to 12 nm in the 6% BZO SD samples. Considering the strain field extends to more than 10 nm from the BZO 1D-APC/YBCO interface,[41] the strain field overlap is present even at the lowest BZO doping of 2 vol.%. Since the strain decreases with increasing distance from the BZO 1D-APC/YBCO interface,[41] a higher strain on the YBCO lattice is anticipated in the BZO SD samples with higher BZO concentrations, which could lead to more defective YBCO lattice, especially via *ab*-plane buckling. This argument seems consistent to the lower T_c values of the BZO SD samples with higher BZO doping at H//ab-plane. However, as we shall discuss more in detail in the following, the formation of defects on the YBCO lattice has a benefit to reduce the strain on the

YBCO, which is consistent with the comparable *c*-axis lattice constants in 4% and 6% BZO SD samples to that of the reference YBCO. Consequently, the strain at the BZO/YBCO interface and hence the interface defects would reduce, which directly impact the pinning efficiency of the BZO 1D-APCs.[31,50] Based on the d values of BZO 1D APCs in the BZO SD samples, the matching field B^* may be estimated from $B^* = \Phi_o/d^2$, assuming a square lattice for the vortices. The B^* values of 5.2 T, 9.2 T and 14.3 T for the 2, 4, and 6% BZO SD samples (Table I) are approximately linearly proportional to the BZO doping. In the 4% BZO DD sample, the d and B^* values are found comparable to that of the 4% BZO SD sample. However, some of the BZO 1D-APCs are no longer through the film thickness due to the presence of the secondary Y_2O_3 3D APCs.[26]

Figure 4 illustrates the $F_p(H)$ curves taken on the 2% (Figures 4a–b), 4% (Figures 4c–d), 6% (Figures 4e–f) BZO SD nanocomposite samples and undoped YBCO samples (Figures 4g–h) at different θ angles of 0°, 22°, 37°, 45°, 67° and 90°. The selection of the θ angles is based on a preliminary test of the $F_p(H)$ curves to ensure the difference between the curves at these angles is
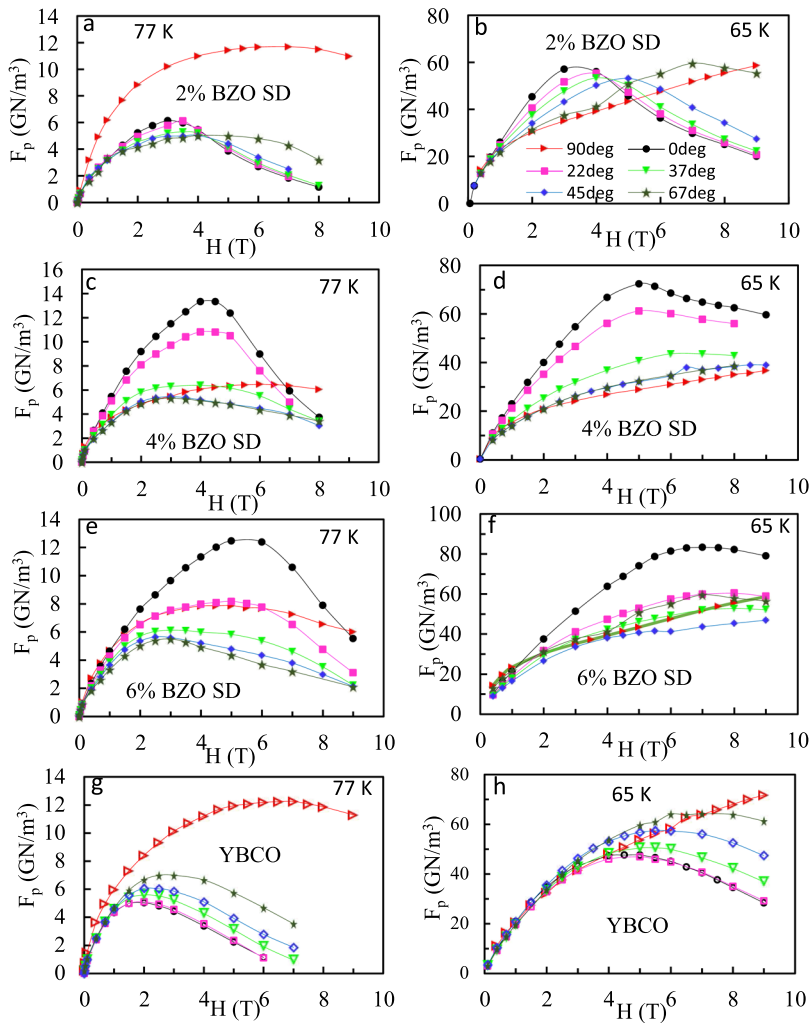

FIG. 4. $F_P(H)$ curves for each θ measured at 77 K (solid symbols) and 65 K (open symbols) on 2% BZO SD (a and b), 4% BZO SD (c and d), 6% BZO SD (e and f) and undoped YBCO (g and h).

not negligible. Two temperatures of 77 K (Figures 4a, c, e, and g) and 65 K (Figures 4b, d, f, and h) were selected considering the interests of applications at or near the liquid nitrogen temperature (77.3 K). At 77 K, an interesting trend of an increasing $F_p(H)$ at $\theta = 0°$ ($H//c$-axis) and lower θ angles can be seen with increasing BZO doping. For example, the $F_p(H)$ curves at lower θ angles below 67° (green star) coincide approximately in the 2% BZO SD sample (Figure 4a) with a comparable peak value $F_{p,max}$ of 5.0-6.1 GN/m³, in contrast to the almost twice as high $F_{p,max}$ at $\theta = 90°$. At a higher BZO doping of 4% (Figure 4c), the $F_p(H)$ curves at $\theta = 0°$ (black) and 22° (purple) outperform that at $\theta = 90°$ and other angles. In particular, the $F_{p,max}$ values for these two angles are both above 10 GN/m³ in contrast to ~ 6 GN/m³ or lower for other angles. It should be realized that this $F_{p,max}$ values are comparable to that due to the *ab*-plane intrinsic pinning shown in Figure 4a. A similar observation is made on 6% BZO SD sample (Figure 4e) with $F_{p,max}$ of 12.5 GN/m³ at $\theta = 0°$ been the highest among all measured at the six θ angles. This result suggests that the pinning efficiency of the BZO 1D-APCs is the lowest in the 2% BZO SD sample. This argument is supported by a similar trend of the $F_p(H)$ curves measured at the same six θ angles on the YBCO reference sample (Figure 4g) at 77 K. In fact, the two samples have similar $F_{p,max}$ values at a specific θ angle, except the location of the $F_{p,max}$, *or* H_{max}, for the 2% BZO SD sample is at a higher magnetic field. This suggests the pinning efficiency of the BZO 1D-APCs in the 2% BZO SD sample is comparable to that of growth defects in YBCO at 77 K. The increased pinning efficiency of the BZO 1D-APCs in BZO/YBCO nanocomposite samples with higher BZO doping may be attributed to the enhanced strain field overlap, which may promote defect formation on the YBCO lattice while reducing the strain at the BZO 1D-APC/YBCO interface and hence minimize the oxygen disorders at such an interface. As we have shown recently in a comparative study of the pinning efficiency of BZO 1D APCs and BHO 1D-APCs of comparable microstructure (lateral dimension and spacing), it is the 1D-APC/YBCO interface that dictates the pinning efficiency.[31] The $F_{p,max}$ values of the BZO 1D-APCs (with

a defective semi-coherent interface with YBCO) could be less than a half of that of the BHO 1D APCs (with a coherent interface with YBCO).

To further illustrate the quantitative difference, the $F_P(H)$ curves of the 2% (Figures 5a–5b) and 4% (Figures 5c–5d) BZO SD samples are overlaid on that for the reference YBCO sample at 77 K and 65 K, respectively. The improvement of the pinning by BZO 1D-APCs is moderate in the 2% SD film relative to the undoped YBCO (Figure 5a) at 77 K. Specifically, only slightly higher $F_{p,max}$ values by about 20% are observed at $\theta = 0°$ and 22°, indicating the pinning efficiency of the BZO 1D-APCs is comparable to that of the growth defects in YBCO. However, an increased H_{max} can be observed from the $F_P(H)$ curves at $\theta = 0°$, 22° and 45°, suggesting an increased total number of pinning centers by the addition of BZO 1D-APCs. Specifically, the H_{max} values at these three orientations for YBCO are 1.5, 2.0 and 2.0 T respectively. These are increased to 3.0, 3.5 and 4.0 T in the 2% SD film, and 4.0, 4.0 and 3.0 T in the 4% SD sample (Figures 5a and 5c). In the 4% SD film, the enhanced $F_{p,max}$ values at 0° and 22° are comparable to the intrinsic pinning value of the reference YBCO illustrating the strong coherence pinning by the BZO 1D-APCs. However, this is at the cost of reduced pinning at $\theta = 90°$, indicative of the defects on the YBCO lattice most probably through ab-plane buckling.

Cantoni *et al* did a careful study on the BZO 1D APC/YBCO interface and revealed a defective BZO/YBCO interface as a column of a few nanometer in thickness surrounding the 1D APC.[41] A possible interface T_c (or T_{cI}) considerably lower than the global T_c of the BZO/YBCO nanocomposite films was suggested based on the TEM data. Considering the pinning efficiency is determined by the APC/YBCO insulator/superconductor interface, a lower pinning efficiency is anticipated for a 1D APC with a more defective BZO/YBCO interface. If indeed the difference in 2% and higher doping BZO SD samples originates from the difference in the BZO/YBCO interface and particularly the lower interface T_{cI}[41] in the 2% SD sample as compared to those of the other nanocomposite
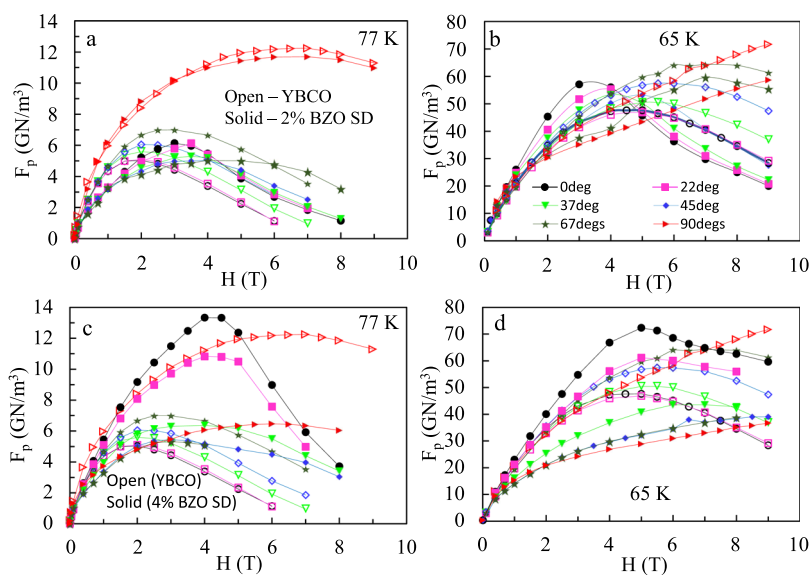

FIG. 5. Comparison of the $F_P(H)$ curves of undoped YBCO (open symbol) with 2% BZO SD (a and b); and 4% BZO SD (c and d) at 77 K and 65 K.

samples, this difference is expected to reduce at the lower temperature of 65 K. This argument is supported by the much enhanced $F_{p,max}$ value of 57.1 GN/m^3 at θ=0° for the 2% SD sample (Figure 4b). While this value is still lower than the $F_{p,max}$ values for 4% (72.4 GN/m^3) and 6% (83.2 GN/m^3) SD samples shown in Figures 4d and 4f respectively, the difference becomes smaller than in the 77 K case. In addition, the strong correlated pinning provided by the BZO 1D-APCs has extended benefits to other orientations of the magnetic field up to θ=37° as shown in Figure 5b for the 2% SD sample and Figure 5d for the 4% SD sample, respectively, in comparison with the undoped YBCO case.

Figures 6a and 6b shows the $F_p(H)$ curves for 4% DD sample at 77 K and 65 K, respectively. The additional Y$_2$O$_3$ 3D APCs in this sample[51,52] has a significant impact on the APC pinning efficiency at different orientations of the magnetic field. At both 77 K and 65 K, the $F_p(H)$ of this sample are lower than its 4% SD counterpart's. This may explain the smaller difference of $F_p(H)$ curves at different magnetic field orientations in the 4% DD film especially at 65 K (Figure 6b) as compared to the more disparate trends of the 4% SD sample (Figure 5d). In addition, a more uniform H_{max} and α values at different H-field orientations are observed in the 4% DD sample (more detailed discussions below). At 77 K, the F_p values of this sample (Figure 6a) are lower than that of its SD counterpart (Figure 5c) at all orientations of the magnetic field. Considering the F_p values become more comparable at 65 K as shown in Figures 6d and 5d, we hypothesis that the 4% DD sample may suffer a similar problem of a significantly reduced T_{cI} at the BZO/YBCO interface to the case of 2% SD sample. Furthermore, unlike the 4% SD case, the 4% DD sample does not show a clear decrease in pinning with increasing θ. In addition, an improvement in the ab-plane pinning can be seen in the 4% DD sample. Specifically, the $F_{p,max}$ value in the 4% DD film is ~ 42 GN/m^3 at θ=90° as opposed to ~ 35 GN/m^3 in the 4% SD film. However, the $F_{p,max}$ values at θ=0° are 73.3 GN/m^3 and 60.2 GN/m^3 in the 4% SD and 4% DD samples

respectively. This reduced correlated pinning in the 4% DD sample might be due to the presence of shorter/segmented BZO 1D-APCs in this sample.

Figures 6c and 6d show an overlay of the $F_p(H)$ curves of the 4% DD sample over those of the reference YBCO. At 77 K, the $F_{p,max}$ values of the YBCO in the range from 5.6 to 12.3 GN/m^3 surpasses those of the 4% DD film in the range of 1.6 to 4.6 GN/m^3 at all H-field orientations (Figure 6c). This clear separation between the two films is altered at 65 K. At θ=0° and 22°, the $F_{p,max}$ for the 4% DD sample out performs the YBCO. For example, θ = 0°, the $F_{p,max}$~60.2 GN/m^3 in the former is considerably higher than the 47.6 GN/m^3 in YBCO. In addition, the benefit of this correlated pinning can be seen to extend to about 22°, but only slightly, with the $F_{p,max}$ (22°) of 46.9 GN/m^3 for YBCO being comparable to $F_{p,max}$ (22°) of 49.5 GN/m^3 for the 4% DD film (Figure 6d). The somewhat reversal of values at these two orientations points to the significance of T_{cI} effect on the pinning abilities of APCs. However, Figures 6c and 6d show that, for the θ range of 37° – 90°, the introduction of 3D APCs does not enhance $F_{p,max}$ to values surpassing those of YBCO. As an illustration, the $F_{p,max}$ values at θ = 90° for the YBCO is more than double that of 4% DD film at 77 K and almost double the DD value at 65 K. This may be attributed to the relative high density of defects in the reference YBCO - as suggested by α ~ 0.30 (Table I) which is lower than the often reported 0.5.[29,30]

The angular range of the effective pinning by the APCs is quantified by the H_{max} (Figure 7a), $F_{p,max}$ (Figure 7b) and α (Figure 7c) values of the nanocomposite films normalized to that of the reference YBCO film as functions of θ at 77 K (solid symbols) and 65 K (open symbols). Among the four nanocomposite samples, a broad angular range of the enhanced H_{max} (over that of the reference YBCO) up to 67° is observed (Figure 7a). In contrast, enhanced $F_{p,max}$ values are observed only in the 4% and 6% SD films in the angular range of 0°–37°. The highest normalized $F_{p,max}$ up to 2.65 is observed on the 4% SD sample at 77 K. This result suggests that
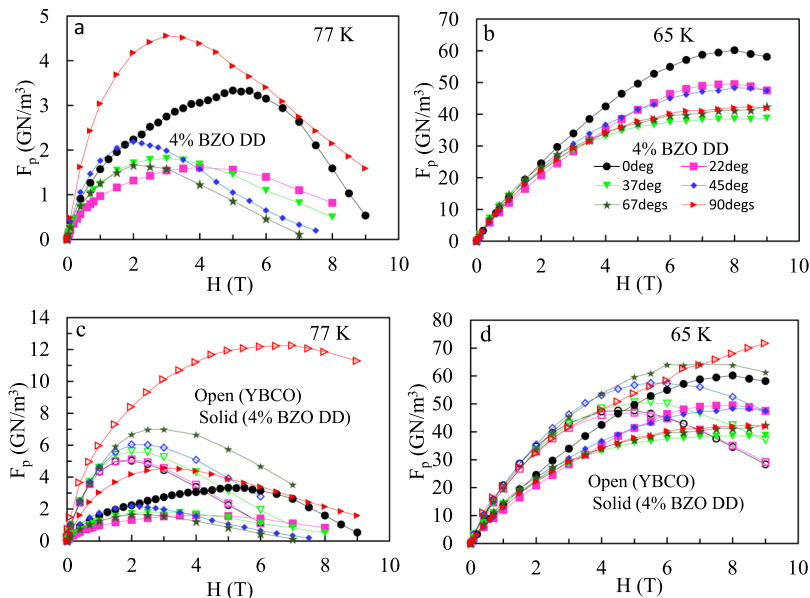

FIG. 6. $F_P(H)$ curves of 4% BZO DD (a) and (b) and comparison with F_P (H) curves of undoped YBCO (open symbol) with 4% BZO DD (c and d) at 77 K and 65 K.
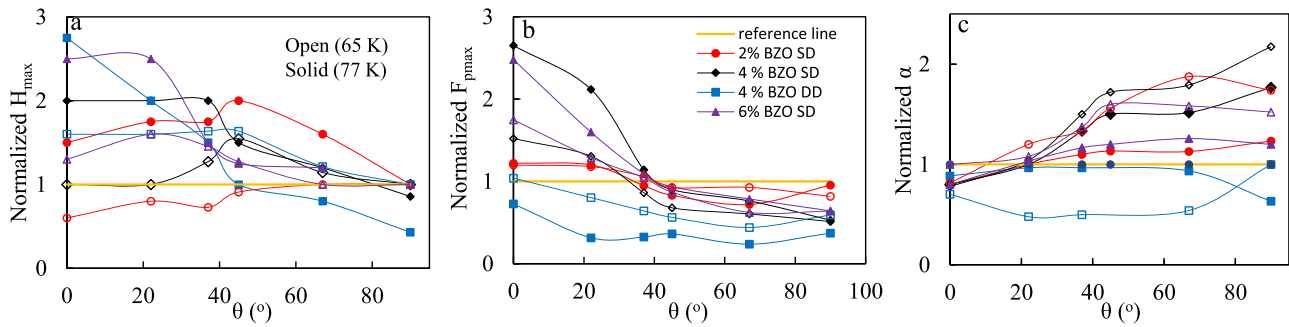
FIG. 7. The ratio of $F_{p,max}$ (a), H_{max}(b) and α (c) to reference YBCO values vs θ at 77 K (solid symbols) and 65 K (open symbols) for the samples- 2% BZO SD (red circle), 4% BZO SD (black diamond), 6% BZO SD (purple triangle) and 4% BZO DD (blue square) with reference line (orange).

while all BZO 1D-APCs provide pinning to vortices, their pinning efficiency may not be uniform even though they have similar morphology. For instance, the BZO 1D-APCs in the 2% SD sample only provide a moderate pinning comparable to that of the growth defects in the undoped YBCO as illustrated in the normalized $F_{p,max}$ ~ 1 almost in the entire range of the θ as shown in Figure 7b. Overall, as illustrated in Figure 7, the 2% SD film has lower enhanced pinning than the 4% and 6% SD samples. This supports the argument that the defective BZO 1D-APC/YBCO interface may have a considerably lower T_{cI} much below that of the nanocomposite film. The BZO 1D-APCs would only provide efficient pinning at temperatures considerably lower than the T_{cI}. In fact, the higher pinning efficiency of the BZO 1D-APCs in 4 and 6% BZO SD samples may be ascribed to the reduction of the tensile strain along the c-axis of YBCO lattice due to the strain field overlap at higher BZO doping, which reduces the BZO/YBCO interface defect concentration and degradation of the T_{cI}. A possible explanation for this can be found in the aforementioned Cantoni $et\ al$ TEM study of strain and defect in BZO/YBCO nanocomposite films.[41] A key observation of this work is the misfit dislocations in a thin YBCO column of a few nm in thickness around the BZO 1D APCs as a consequence of the global strain due to lattice mismatch at the BZO/YBCO interface. In this column, the local strain is much reduced from that of the global strain due to the formation of the defects together with significant oxygen deficiency. Since the global strain field extends to 10-12 nm away from the BZO/YBCO interface, strain field overlapping occurs even at the lowest BZO doping of 2 vol.% in this work - considering the inter-BZO 1D APC (center-to-center) is around 20 nm that translates to the BZO 1D APC (of diameter of~ 6 nm) surface-to-surface distance of YBCO around 14 nm. With increasing BZO doping and hence decreasing inter-1D APC spacing, a further increased strain field overlap results in formation of defects also in YBCO matrix which is consistent with the less expanded c-axis lattice constants at higher BZO concentrations as shown in the XRD data. This leads to two opposite effects on the pinning efficiency of the BZO 1D APCs: a possible reduction of the defect concentration in the column surrounding the BZO 1D APC (hence less degraded T_{cI}) and a further reduction of global T_c of the BZO/YBCO nanocomposites. The compromise of these two opposite effects may explain the optimal pinning in the 4 vol.% BZO SD sample, especially the wider angular range of pinning enhancement of the 4% BZO SD film as compared

to the 2% and 6% SD counterparts. On the other hand, the mixed APC morphologies in the 4% BZO DD film provide benefit of low α value in a wide range up to 67° (Figure 7c) and the enhanced normalized H_{max} in the comparable angular range, despite the overall lower $F_p(H)$.

IV. CONCLUSION

In summary, transport $J_c(H)$ curves, and the calculated $F_p(H)$ curves, at different H-field orientations, have been utilized to determine the angular range of the pinning efficiency of c-axis aligned 1D-BZO APCs in APC/YBCO nanocomposite films. These films include BZO SD samples with BZO doping in the range of 2-6 vol.%, and a 4% DD sample that contains 4 vol.% BZO+3 vol.% Y_2O_3. An undoped YBCO sample was also included in the study as the reference for evaluation of the APC pinning efficiency. The $F_{p,max}$, H_{max}, and the α values are obtained as functions of θ for the nanocomposite films. By normalizing them to the corresponding values of the reference YBCO sample, we aim to elucidate a quantitative correlation between the pinning efficiency of individual 1D APCs and the effective angular range at 65 K and 77 K, respectively. Several insights have been obtained in this study. First, most nanocomposite samples have normalized $H_{max} > 1$ over a larger angular range up to ~ 67°, indicating both 1D and 3D APCs could add additional pinning centers to YBCO. However, normalized $F_{p,max} > 1$ were only observed in 4% and 6% BZO SD samples in the angular range of 0-37°. The highest normalized $F_{p,max}$ ~ 2.65 can be observed in 4% SD sample at θ =0 ° and 77 K. In contrast, the normalized $F_{p,max}$ ~ 1 in the 2% SD sample at both temperatures while it is less than 1 in 4% DD sample. This result reveals that the pinning efficiency of BZO 1D-APCs may be sensitively affected by the BZO/YBCO interface because of the strain field overlap at different BZO doping levels. The more intensive strain field overlap at higher BZO doping due to a smaller inter 1D APC spacing may directly generate defects on YBCO lattice and consequently reduces the BZO/YBCO interface strain and defect concentration. This in turn reduces degradation of the T_{cI} at the interface and leads to higher pinning efficiency, resulting in normalized $F_{p,max}$ value > 1 in a wide angular range. Nevertheless, the low and uniform α values in the 4% DD sample indicate its effectiveness as an isotropic pinning landscape across the entire θ range.

REFERENCES

[1] T. Matsushita, "Flux pinning in superconducting 123 materials," Superconductor Science & Technology **13**(6), 730–737 (2000).

[2] K. Matsumoto and P. Mele, "Artificial pinning center technology to enhance vortex pinning in YBCO coated conductors," Superconductor Science and Technology **23**(1), 014001 (2009).

[3] J. MacManus-Driscoll, S. Foltyn, Q. Jia, H. Wang, A. Serquis, L. Civale, B. Maiorov, M. Hawley, M. Maley, and D. Peterson, "Strongly enhanced current densities in superconducting coated conductors of YBa$_2$Cu$_3$O$_{7-x}$+BaZrO$_3$," Nature Materials **3**(7), 439 (2004).

[4] J. J. Shi and J. Z. Wu, "Micromechanical model for self-organized secondary phase oxide nanorod arrays in epitaxial YBa$_2$Cu$_3$O$_{7-\delta}$ films," Philosophical Magazine **92**(23), 2911–2922 (2012).

[5] J. Wu and J. Shi, "Interactive modeling-synthesis-characterization approach towards controllable in situ self-assembly of artificial pinning centers in RE-123 films," Superconductor Science and Technology **30**(10), 103002 (2017).

[6] F. Baca, P. Barnes, R. Emergo, T. Haugan, J. Reichart, and J. Wu, "Control of BaZrO$_3$ nanorod alignment in YBa$_2$Cu$_3$O$_{7-x}$ thin films by microstructural modulation," Applied Physics Letters **94**(10), 102512 (2009).

[7] F. J. Baca, T. J. Haugan, P. N. Barnes, T. G. Holesinger, B. Maiorov, R. Lu, X. Wang, J. N. Reichart, and J. Z. Wu, "Interactive growth effects of rare-earth nanoparticles on nanorod formation in YBa$_2$Cu$_3$O$_x$ thin films," Advanced Functional Materials **23**(38), 4826–4831 (2013).

[8] R. Emergo, F. Baca, J. Wu, T. Haugan, and P. Barnes, "The effect of thickness and substrate tilt on the BZO splay and superconducting properties of YBa$_2$Cu$_3$O$_{7-\delta}$ films," Superconductor Science and Technology **23**(11), 115010 (2010).

[9] A. Goyal, S. Kang, K. J. Leonard, P. M. Martin, A. A. Gapud, M. Varela, M. Paranthaman, A. O. Ijaduola, E. D. Specht, and J. R. Thompson, "Irradiation-free, columnar defects comprised of self-assembled nanodots and nanorods resulting in strongly enhanced flux-pinning in YBa$_2$Cu$_3$O$_{7-\delta}$ films," Superconductor Science and Technology **18**(11), 1533 (2005).

[10] P. Mele, K. Matsumoto, T. Horide, A. Ichinose, M. Mukaida, Y. Yoshida, S. Horii, and R. Kita, "Ultra-high flux pinning properties of BaMO$_3$-doped YBa$_2$Cu$_3$O$_{7-x}$ thin films (M= Zr, Sn)," Superconductor Science and Technology **21**(3), 032002 (2008).

[11] X. Wang, F. J. Baca, R. L. Emergo, J. Z. Wu, T. J. Haugan, and P. N. Barnes, "Eliminating thickness dependence of critical current density in YBa$_2$Cu$_3$O$_{7-x}$ films with aligned BaZrO$_3$ nanorods," Journal of Applied Physics **108**(11), 113911 (2010).

[12] D. Feldmann, T. Holesinger, B. Maiorov, S. Foltyn, J. Coulter, and I. Apodaca, "Improved flux pinning in YBa$_2$Cu$_3$O$_7$ with nanorods of the double perovskite Ba$_2$YNbO$_6$," Superconductor Science and Technology **23**(9), 095004 (2010).

[13] S. Harrington, J. Durrell, B. Maiorov, H. Wang, S. Wimbush, A. Kursumovic, J. Lee, and J. MacManus-Driscoll, "Self-assembled, rare earth tantalate pyrochlore nanoparticles for superior flux pinning in YBa$_2$Cu$_3$O$_{7-\delta}$ films," Superconductor Science and Technology **22**(2), 022001 (2008).

[14] C. Varanasi, J. Burke, H. Wang, J. Lee, and P. Barnes, "Thick YBa$_2$Cu$_3$O$_{7-x}$+ BaSnO$_3$ films with enhanced critical current density at high magnetic fields," Applied Physics Letters **93**(9), 092501 (2008).

[15] S. H. Wee, A. Goyal, Y. L. Zuev, C. Cantoni, V. Selvamanickam, and E. D. Specht, "Formation of self-assembled, double-perovskite, Ba$_2$YNbO$_6$ nanocolumns and their contribution to flux-pinning and Jc in Nb-Doped YBa$_2$Cu$_3$O$_{7-\delta}$ films," Applied Physics Express **3**(2), 023101 (2010).

[16] M. Sieger, J. Hänisch, P. Pahlke, M. Sparing, U. Gaitzsch, K. Iida, R. Nast, E. Reich, L. Schultz, and B. Holzapfel, "BaHfO$_3$-Doped Thick YBa$_2$Cu$_3$O$_{7-\delta}$ films on highly alloyed textured Ni-W tapes," IEEE Transactions on Applied Superconductivity **25**(3), 1–4 (2015).

[17] M. Sieger, P. Pahlke, J. Hänisch, M. Sparing, M. Bianchetti, J. MacManus-Driscoll, M. Lao, M. Eisterer, A. Meledin, and G. Van Tendeloo, "Ba$_2$Y(Nb/Ta)O$_6$– Doped YBCO films on biaxially textured Ni–5at.% W substrates," IEEE Transactions on Applied Superconductivity **26**(3), 1–5 (2016).

[18] S. Chen, M. A. Sebastian, B. Gautam, J. Wilt, T. Haugan, Z. Xing, and J. Wu, "Enhancement of isotropic pinning force in YBCO films with BaZrO$_3$ nanorods and Y$_2$O$_3$ nanoparticles," IEEE Trans. Appl. Supercond. **27**(4), 1 (2017).

[19] G. Ercolano, M. Bianchetti, S. Wimbush, S. Harrington, H. Wang, J. Lee, and J. MacManus-Driscoll, "State-of-the-art flux pinning in YBa$_2$Cu$_3$O$_{7-\delta}$ by the creation of highly linear, segmented nanorods of Ba$_2$(Y/Gd)(Nb/Ta)O$_6$ together with nanoparticles of (Y/Gd)$_2$O$_3$ and (Y/Gd) Ba$_2$Cu$_4$O$_8$," Superconductor Science and Technology **24**(9), 095012 (2011).

[20] T. Horide, T. Kawamura, K. Matsumoto, A. Ichinose, M. Yoshizumi, T. Izumi, and Y. Shiohara, "Jc improvement by double artificial pinning centers of BaSnO$_3$ nanorods and Y$_2$O$_3$ nanoparticles in YBa$_2$Cu$_3$O$_7$ coated conductors," Superconductor Science and Technology **26**(7), 075019 (2013).

[21] A. K. Jha, K. Matsumoto, T. Horide, S. Saini, P. Mele, A. Ichinose, Y. Yoshida, and S. Awaji, "Controlling the critical current anisotropy of YBCO superconducting films by incorporating hybrid artificial pinning centers," IEEE Transactions on Applied Superconductivity **26**(3), 1–4 (2016).

[22] A. K. Jha, K. Matsumoto, T. Horide, S. Saini, P. Mele, Y. Yoshida, and S. Awaji, "Systematic variation of hybrid APCs into YBCO thin films for improving the vortex pinning properties," IEEE Transactions on Applied Superconductivity **25**(3), 1–5 (2015).

[23] B. Maiorov, S. Baily, H. Zhou, O. Ugurlu, J. Kennison, P. Dowden, T. Holesinger, S. Foltyn, and L. Civale, "Synergetic combination of different types of defect to optimize pinning landscape using BaZrO$_3$-doped YBa$_2$Cu$_3$O$_7$," Nature materials **8**(5), 398 (2009).

[24] K. Matsumoto, T. Horide, A. K. Jha, P. Mele, Y. Yoshida, and S. Awaji, "Irreversibility fields and critical current densities in strongly pinned YBa$_2$Cu$_3$O$_{7-x}$ films with artificial pinning centers," IEEE Transactions on Applied Superconductivity **25**(3), 1–6 (2015).

[25] W. Buckel and R. Kleiner, *Superconductivity: Fundamentals and applications* (John Wiley & Sons, 2008).

[26] S. Chen, M. A. Sebastian, B. Gautam, J. Wilt, Y. Chen, L. Sun, Z. Xing, T. Haugan, and J. Wu, "Generating mixed morphology BaZrO$_3$ artificial pinning centers for strong and isotropic pinning in BaZrO$_3$–Y$_2$O$_3$ double-doped YBCO thin films," Superconductor Science and Technology **30**(12), 125011 (2017).

[27] B. Gautam, M. A. Sebastian, S. Chen, T. Haugan, Y. Chen, Z. Xing, J. Prestigiacomo, M. Osofsky, and J. Wu, "Towards isotropic vortex pinning in YBCO films with double-doping BHO-Y$_2$O$_3$ and BZO-Y$_2$O$_3$ artificial pining centers," IOP Conference Series: Materials Science and Engineering **279**, 012030 (2017).

[28] B. Gautam, M. A. Sebastian, S. Chen, T. Haugan, W. Zhang, J. Huang, H. Wang, and J. Z. Wu, "Microscopic adaptation of BaHfO$_3$ and Y$_2$O$_3$ artificial pinning centers for strong and isotropic pinning landscape in YBa$_2$Cu$_3$O$_{7-x}$ thin films," Superconductor Science and Technology **31**(2), 025008 (2018).

[29] J. J. Shi and J. Z. Wu, "Influence of the lattice strain decay on the diameter of self assembled secondary phase nanorod array in epitaxial films," Journal of Applied Physics **118**(16), 164301 (2015).

[30] J. Wu, J. Shi, F. Baca, R. Emergo, J. Wilt, and T. Haugan, "Controlling BaZrO$_3$ nanostructure orientation in YBa$_2$Cu$_3$O films for a three-dimensional pinning landscape," Superconductor Science and Technology **28**(12), 125009 (2015).

[31] B. Gautam, M. A. Sebastian, S. Chen, S. Misra, J. Huang, F. Javier Baca, R. Emergo, T. Haugan, Z. Xing, and H. Wang, "Probing the effect of interface on vortex pinning efficiency of one-dimensional BaZrO$_3$ and BaHfO$_3$ artificial pinning centers in YBa$_2$Cu$_3$O$_{7-x}$ thin films," Applied Physics Letters **113**(21), 212602 (2018).

[32] L. Civale, B. Maiorov, A. Serquis, J. Willis, J. Coulter, H. Wang, Q. Jia, P. Arendt, J. a. MacManus-Driscoll, and M. Maley, "Angular-dependent vortex pinning mechanisms in YBa$_2$Cu$_3$O$_7$ coated conductors and thin films," Applied Physics Letters **84**(12), 2121–2123 (2004).

[33] S. R. Foltyn, H. Wang, L. Civale, B. Maiorov, and Q. Jia, "The role of interfacial defects in enhancing the critical current density of YBa$_2$Cu$_3$O$_{7-\delta}$ coatings," Superconductor Science and Technology **22**(12), 125002 (2009).

[34] B. Maiorov, "A new scaling approach and quantitative angular critical current measurement using magnetization," Superconductor Science and Technology **29**(3), 030501 (2016).

[35] B. Maiorov, S. Baily, Y. Kohama, H. Hiramatsu, L. Civale, M. Hirano, and H. Hosono, "Angular and field properties of the critical current and melting line of Co-doped SrFe$_2$As$_2$ epitaxial films," Superconductor Science and Technology **22**(12), 125011 (2009).

[36] B. Maiorov, B. Gibbons, S. Kreiskott, V. Matias, Q. Jia, T. Holesinger, and L. Civale, "Influence of tilted geometries on critical current in superconducting thin films," IEEE Transactions on Applied Superconductivity **15**(2), 2582–2585 (2005).

[37] B. Maiorov, A. Kursumovic, L. Stan, H. Zhou, H. Wang, L. Civale, R. Feenstra, and J. MacManus-Driscoll, "Vortex pinning landscape in YBa$_2$Cu$_3$O$_7$ films grown by hybrid liquid phase epitaxy," Superconductor Science and Technology **20**(9), S223 (2007).

[38] B. Maiorov, H. Wang, S. Foltyn, Y. Li, R. DePaula, L. Stan, P. Arendt, and L. Civale, "Influence of naturally grown nanoparticles at the buffer layer in the flux pinning in YBa$_2$Cu$_3$O$_7$ coated conductors," Superconductor Science and Technology **19**(9), 891 (2006).

[39] A. A. Gapud, D. Kumar, S. Viswanathan, C. Cantoni, M. Varela, J. Abiade, S. J. Pennycook, and D. K. Christen, "Enhancement of flux pinning in YBa$_2$Cu$_3$O$_{7-\delta}$ thin films embedded with epitaxially grown Y$_2$O$_3$ nanostructures using a multi-layering process," Superconductor Science and Technology **18**(11), 1502 (2005).

[40] P. Mele, K. Matsumoto, T. Horide, A. Ichinose, M. Mukaida, Y. Yoshida, S. Horii, and R. Kita, "Incorporation of double artificial pinning centers in YBa$_2$Cu$_3$O$_{7-d}$ films," Superconductor Science and Technology **21**(1), 015019 (2007).

[41] C. Cantoni, Y. Gao, S. H. Wee, E. D. Specht, J. Gazquez, J. Meng, S. J. Pennycook, and A. Goyal, "Strain-driven oxygen deficiency in self-assembled, nanostructured, composite oxide films," ACS Nano **5**(6), 4783–4789 (2011).

[42] M. A. Sebastian, C. Ebbing, W. Zhang, J. Huang, H. Wang, S. Chen, B. Gautum, J. Wu, and T. Haugan, "Comparison study of the flux pinning enhancement of YBCO superconductor with BZO and BZO + Y$_2$O$_3$ mixed phase additions," IOP Conference Series: Materials Science and Engineering **279**, 012031 (2017).

[43] M. A. P. Sebastian, J. N. Reichart, M. M. Ratcliff, T. J. Bullard, J. L. Burke, C. R. Ebbing, G. Y. Panasyuk, C. Tsai, W. Zhang, J. Huang, H. Wang, J. Wu, and T. J. Haugan, "Study of the flux pinning landscape of YBCO thin films with single and mixed phase additions BaMO$_3$ + Z: M = Hf, Sn, Zr and Z = Y$_2$O$_3$, Y$_{211}$," IEEE Transactions on Applied Superconductivity **27**(4), 1–5 (2017).

[44] B. Gautam, M. A. Sebastian, S. Chen, J. Shi, T. Haugan, Z. Xing, W. Zhang, J. Huang, H. Wang, and M. Osofsky, "Transformational dynamics of BZO and BHO nanorods imposed by Y$_2$O$_3$ nanoparticles for improved isotropic pinning in YBa$_2$Cu$_3$O$_{7-\delta}$ thin films," AIP Advances **7**(7), 075308 (2017).

[45] R. L. S. Emergo, PhD Thesis, "Enhancing Jc (B, theta) in YBa$_2$Cu$_3$O$_7$-delta via nano-engineering of pinning structures," University of Kansas, 2009.

[46] B. A. Malik, M. A. Malik, and K. Asokan, "Optimization of BaZrO$_3$ concentration as secondary phase in superconducting YBa$_2$Cu$_3$O$_7$ for high current applications," AIP Advances **6**(4), 045317 (2016).

[47] B. Gautam, S. Chen, M. A. Sebastian, T. Haugan, Z. Xing, and J. Wu, "Mixed artificial pining centers by single-doping BaZrO$_3$ and double-doping BaZrO$_3$ +Y$_2$O$_3$ YBa$_2$Cu$_3$O$_{7-x}$ on flat and vicinal substrates," IEEE Transactions on Applied Superconductivity **28**(4), 1–4 (2018).

[48] J. Z. Wu, J. F. Baca, J. J. Shi, R. Emergo, T. J. Haugan, B. Maiorov, and T. Holesinger, "The effect of lattice strain on the diameter of BaZrO$_3$ nanorods in epitaxial YBa$_2$Cu$_3$O$_{7-d}$ films," Superconductor Science & Technology **27**, 044010 (2014).

[49] J. J. Shi and J. Z. Wu, "Influence of the lattice strain decay on the diameter of self assembled secondary phase nanorod array in epitaxial films," Journal of Applied Physics **118**(16), 164301 (2015).

[50] J. Wu, G. Bibek, M. A. Sebastian, V. Ogunjimi, T. Haugan, J. Huang, S. Misra, F. J. Baca, J. C. Prestigiacomo, H. Wang, and M. Osofsky, "Pinning efficiency of one-dimensional artificial pinning centers in YBa$_2$Cu$_3$O$_{7-x}$ thin films," IEEE Transactions on Applied Superconductivity **29**, 1 (2019).

[51] B. Gautam, S. H. Chen, M. A. Sebastian, T. Haugan, Z. W. Xing, and J. Wu, "Mixed artificial pining centers by single-doping BaZrO$_3$ and double-doping BaZrO$_3$+Y$_2$O$_3$ YBa$_2$Cu$_3$O$_{7-x}$ on flat and vicinal substrates," IEEE Transactions on Applied Superconductivity **28**(4), 1–4 (2018).

[52] B. Gautam, M. A. Sebastian, S. Chen, T. J. Haugan, W. Zhang, J. Huang, H. Wang, and J. Z. Wu, "Microscopic adaptation of BaHfO$_3$ and Y$_2$O$_3$ artificial pinning centers for strong and isotropic pinning landscape in YBa$_2$Cu$_3$O$_{7-x}$ thin films," Superconductor Science and Technology **31**, 025008 (2018).